

# We are IntechOpen, the world's leading publisher of Open Access books Built by scientists, for scientists

6,900

Open access books available

186,000

International authors and editors

200M

Downloads

Our authors are among the

154

Countries delivered to

TOP 1%

most cited scientists

12.2%

Contributors from top 500 universities



WEB OF SCIENCE™

Selection of our books indexed in the Book Citation Index  
in Web of Science™ Core Collection (BKCI)

Interested in publishing with us?  
Contact [book.department@intechopen.com](mailto:book.department@intechopen.com)

Numbers displayed above are based on latest data collected.  
For more information visit [www.intechopen.com](http://www.intechopen.com)



# Surface-Enhanced Raman Spectroscopy (SERS) Based on ZnO Nanorods for Biological Applications

*Sanghwa Lee and Jun Ki Kim*

## Abstract

Detection of nanometer-sized biomarkers is a research topic that attracts much attention as an application for early diagnosis of diseases. Biopsy monitoring by analyzing cell secretion in a non-destructive way has many advantages in the field of biomedicine. We introduce the Raman signal enhancement method on a bio-sensing chip based on surface-enhanced Raman diagnosis. This approach has the advantage because the ZnO nanorods are grown to form nanoscale porosity and are coated with gold to enable size selective biomarker detection. After sputtering gold on the grown ZnO nanostructures, the unique feature of clustering the nanorod's heads first appeared. The grain formation on the head was the main factor for the localized surface plasmon resonance (LSPR) enhancement, and this fact could be verified by finite element analysis. It has been demonstrated in breast cancer cell line that the cell viability is also high in such gold-clad ZnO nanostructure-based surface-enhanced substrates. For bioapplication, interstitial cystitis/bladder pain syndrome (IC/BPS) animal model was prepared by injecting HCl into the bladder of a rat, and urine was collected a week later to conduct Raman spectroscopy experiments.

**Keywords:** surface-enhanced Raman spectroscopy (SERS), ZnO nanorods, gold clustering, finite element method (FEM), cell viability, interstitial cystitis/bladder pain syndrome (IC/BPS)

## 1. Introduction

Biological particles on the nanometer and submicrometer scale, such as proteins, lipids, nucleic acids, exosomes, and metabolic content, have attracted much attention as biomarkers for diagnosing diseases from biologically generated fluids such as blood, urine, and lymph. These biomarkers are now understood to be fundamental to healthy intercellular communication and can be produced in diseased cells. Label free Raman spectroscopy is useful for verification of biological samples ranging from nanoscale to millimeter size, such as tissue [1, 2], cells [3–5], bacteria [6, 7], exosomes [8, 9], and proteins [10, 11]. After incident laser emission with a single wavelength, Raman spectroscopy can identify biomarkers with the spectral peak position as a fingerprint because the molecular vibrations of the sample are

represented by spectra due to inelastic scattering. Electromagnetic enhancement can be achieved on rough surface of metal such as a gold or silver nanoparticle that causes amplification of the light by local surface plasmon resonance (LSPR) effects [12, 13].

A “hot spot” is formed on the surface of the SERS particles, and the Raman signal is dramatically increased at the nano-sized gap. Surface-enhanced Raman spectroscopy (SERS) is an approach for cell analysis and identification that applies a wide range of chemical spectroscopy to nanometer-sized biomarkers. Recent studies on monomolecular scales have been made possible through surface-enhanced Raman techniques [14–18]. According to finite element method (FEM) analysis, when the colloid is separated by 2 nm between a diameter of 30 nm colloids, a “hot spot” is formed which gives a surface-enhanced effect of about  $10^8$  degrees [13]. In biomedical applications, biomarkers suitable for these nanogaps are very rare, and due to the size and shape of biomolecules, research on nanogap and signal enhancement of the SERS structure is needed to optimize the LSPR effect.

In this chapter, we fabricated SERS substrate based on ZnO nanorods and improved the SERS effect by forming selective growth clustering of gold nanoparticles, which could be formed in specific condition of ZnO nanorod-based SERS substrate. To control the porosity and gold nanostructure, the length and density of the ZnO nanostructures and the thickness of the deposited gold were modified morphologically. The SERS enhancement mechanism was described based on finite element analysis. Cell viability was also evaluated to determine the presence or absence of toxicity for cancer cell applications. In other bio-applications, we demonstrate early diagnostic possibilities with Raman signals and statistical analyses from nano-sized biomarkers of intractable inflammatory diseases that cause patient pain.

## **2. Nanorod manufacturing method**

Most of the research to fabricate SERS-based chips focuses on optimizing the surface of substrates through nanomaterials and nanostructures synthesized using sophisticated techniques such as lithographic patterning or high-temperature processes [16, 19–22]. Other research groups deposit Au/Ag nanoparticles on papers [23–25] or coat metal on a Si nanowire structure [26] to make a porous SERS substrate suitable for biological or liquid samples. Such Si nanowires are too dependent on the substrate and are difficult to combine with common cell culture substrates such as glass and petri dishes, due to their amorphous and manufacturing nature. In the case of paper-based SERS substrate, porosity and nanogaps could not be adjusted. On the other hand, if a ZnO nanorod-based platform is introduced, the substrate can be manufactured at a temperature below 100°C. Furthermore, homogeneous nanostructures can be formed without any lithography process on amorphous substrates such as glass and plastic, which are common in bioscience applications [27, 28].

To make the SERS substrates, the Si wafer were scribed with a size of  $1 \times 1 \text{ cm}^2$  for substrate of ZnO nanorods initially. It was cleaned in ethanol and deionized (DI) water for 5 min, respectively. The 30 nm ZnO seed layer was deposited on the surface of as-prepared samples by using RF magnetron sputtering for 5 min under 100 W power to grow the vertically aligned ZnO nanorods utilizing by the hydrothermal synthesis. The ZnO growth solution was prepared by dissolving 10 mM zinc nitrate hexahydrate (Sigma-Aldrich Co.) and 0.9 mL of ammonium hydroxide (Sigma-Aldrich Co.) in 30 mL DI water. A homogeneous aqueous solution was achieved using mildly stirred vortexer for 5 min at room temperature. Then, the as-prepared samples were immersed into the aqueous solution in an oven at 90°C for 50 min.

### 3. SERS metal growth and enhancement test

After ZnO growth, the substrates were cleaned with DI water and dried with nitrogen gas. Finally, the ZnO nanorods (NRs) were coated with Au using a thermal evaporator (Alpha Plus Co., Ltd., Korea). The thickness monitor for 100 and 200 nm deposition was standardized. The morphological and structural properties of the Raman measured samples were observed by using a field-emission scanning electron microscope (FE-SEM) (S-4700, HITACHI, Japan) with 15 kV beam voltage. The procedure of the experiment including the measurement analysis is schematically shown as a diagram in **Figure 1**.

To obtain adequate porosity for the solution sample, the ZnO seed layer was modified and deposited such that the preferential growth direction of the zinc oxide nanorods was within about  $10^\circ$  from vertical. A volume of gold having a height of 100 and 200 nm per unit area was deposited on nanorods having length distribution of 300–450 nm or 500–650 nm, respectively. These four specimens were displayed with FE-SEM images of the  $45^\circ$  tilt view as shown in **Figure 2**. The top and bottom of the **Figure 2e** show the substrates with gold deposited (top) and not deposited (bottom) for **Figure 2a**, and ZnO is fully covered even when only 100 nm of gold is deposited. When the gold deposition is increased to 200 nm, the rod thickness is distributed about 10–30 nm thicker than when the gold deposition is not performed. Also, since the nanorod length distribution has a standard deviation of 50 nm and the deposited gold is clustered at the head of the nanorods, the height distribution of the gold clusters undergoes a similar variation. Therefore, when confocal Raman spectroscopy measurements are focused on the gold clusters, the head size can be a key factor in the Raman enhancement effect.

The Raman enhancement effect of SERS substrate based on ZnO nanorods was confirmed using 1 mM Rhodamine B drop, and the signals were measured after natural drying. Rhodamine B (RhB, >95%) purchased from Sigma-Aldrich was used as a standard for Raman measurements due to its refined condition. Raman measurements (LabRam Aramis, Horiba) were carried out using a 785 nm diode laser in a confocal geometry with a 0.5 NA, x50 objective lens and beam spot diameter  $\sim 1.9 \mu\text{m}$ . The spectrum of each point was measured in the range of  $400\text{--}2500 \text{ cm}^{-1}$  with a spectral resolution of  $5 \text{ cm}^{-1}$  and an integration time of 30 s at room

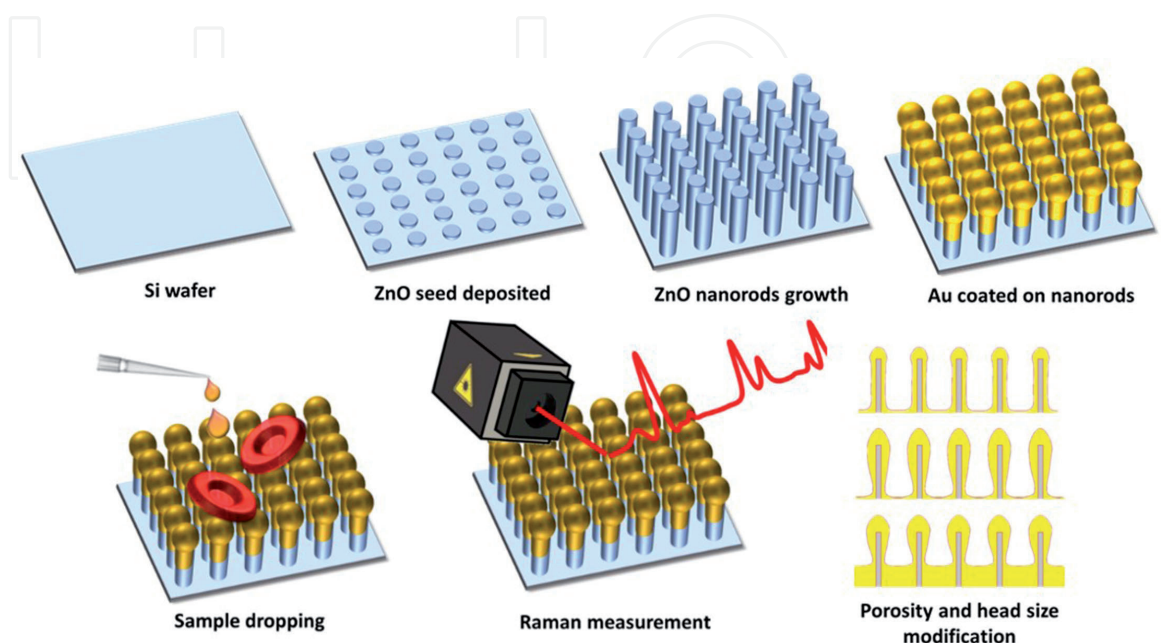


**Figure 1.** Schematic of the experiment involving zinc oxide nanostructure-based SERS substrate fabrication.

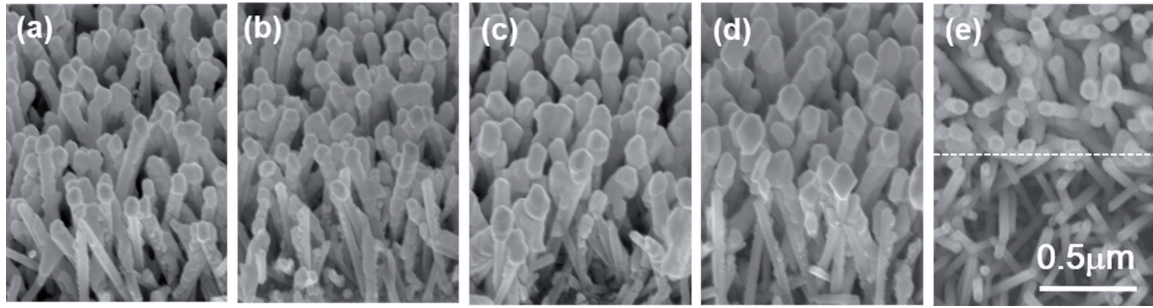


**Figure 2.** Secondary electron images of the substrate with nanorod length and deposited gold thickness modified for (a) ZnO of length 400 nm with 100 nm deposited Au, (b) 600 nm length ZnO with 100 nm Au, (c) 400 nm length ZnO with 200 nm Au, and (d) 400 nm ZnO with 200 nm Au. (e) Shows the initial difference in covering due to gold coating. All of scales are the same.

temperature. The spectra were postprocessed by Savitzky-Golay smoothing, and a third-order polynomial fit to the autofluorescence background was subtracted.

**Figure 3a** shows the enhancement of the Raman signal ranging from 1000 to 1500  $\text{cm}^{-1}$  according to each specimen. The greatest enhancement was observed in 600 nm ZnO nanorods deposited with 200 nm gold, which is a correction to the area of the circle by drying droplet. However, without area correction, a random point of 400 nm in length with the same average gold thickness appeared to give a greater improvement. This difference is explained by the correlation between signal enhancement and sample concentration. The enhancement factor EF follows the equation:

$$EF = \left( \frac{I_{\text{SERS}}}{I_{\text{bare}}} \right) \left( \frac{C_{\text{bare}}}{C_{\text{SERS}}} \right)$$

where  $C_{\text{SERS}}$  is the concentration of RhB on the ZnO nanorod-coated Au SERS substrate,  $I_{\text{SERS}}$  is the measured Raman intensity from the nanorod-coated substrate, and  $C_{\text{bare}}$  and  $I_{\text{bare}}$  are the same quantities on the bare substrate, respectively. The effective concentration of RhB on the dried specimen varies across the sample as the diffusion of the droplet depends upon the porosity of the SERS substrate. In addition, even though samples of the same volume are dropped for all experiments, the value of  $C_{\text{bare}}/C_{\text{SERS}}$  is dependent upon a correction for area since the initial droplet varies in size. Therefore, EF due to the substrate correction can be seen to be largest in the 200 nm gold-coated nanorods of 600 nm length. This enhancement is independent for each specific peak, as shown in **Figure 3b**. This measurement shows that the enhancement effect is compared without denaturation of the sample, since the relative ratio between the peaks does not change significantly.

In addition, the SERS substrates based on zinc oxide nanorods show no coffee ring effect, as shown in **Figure 3c**. Due to the rise in concentration at the ring region, the edges of RhB on bare substrates and of RhB on gold thin films show stronger Raman signals. On the other hand, nanorod substrates have larger values in the interior of the deposition ring as shown in **Figure 3d**.

#### 4. Localized surface plasmon resonance (LSPR) analysis

Calculation analysis using FEM was performed to understand the effect of Au cluster size on SERS enhancement. The finite element method (FEM) was used in COMSOL Multiphysics software (COMSOL Inc., USA) to simulate the SERS activities of the electromagnetic fields. A two-dimensional model for metal-coated

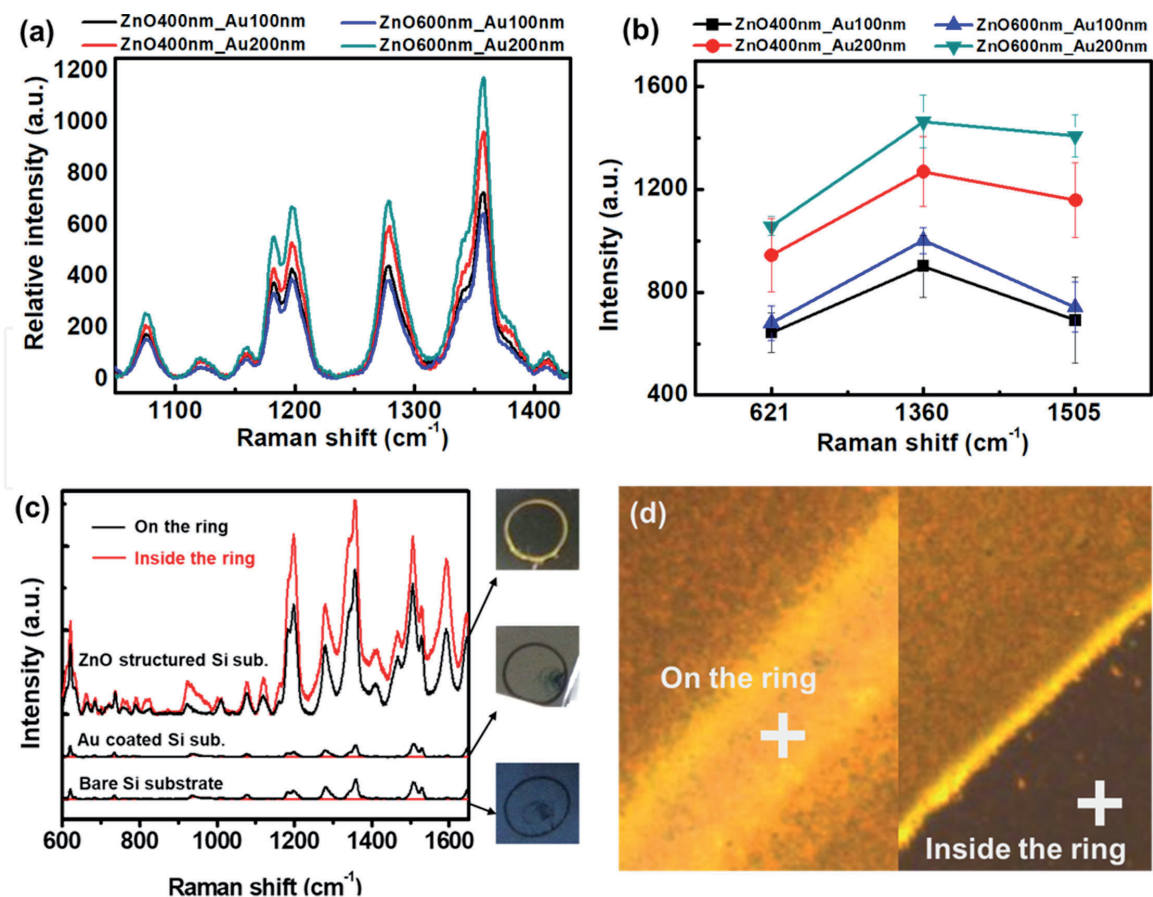


**Figure 3.** (a) Raman signal enhancement of RhB on each substrate. (b) Differences in the enhancement intensity of each specific peak according to the substrate. (c) Differences in the coffee ring effect of the Raman signal depending on the nanostructure. (d) Optical microscope image including Raman acquired point.

nanostructured substrates with various metal spherical diameters has been established. The near-field distribution of the electromagnetic field was calculated for given boundary condition to solve the equation of time harmonic Maxwell at the excitation wavelength of 785 nm.

From secondary electron microscopy images, structures were modeled with 80 and 125 nm heads on nanorods of width 50 nm including gold coating and length

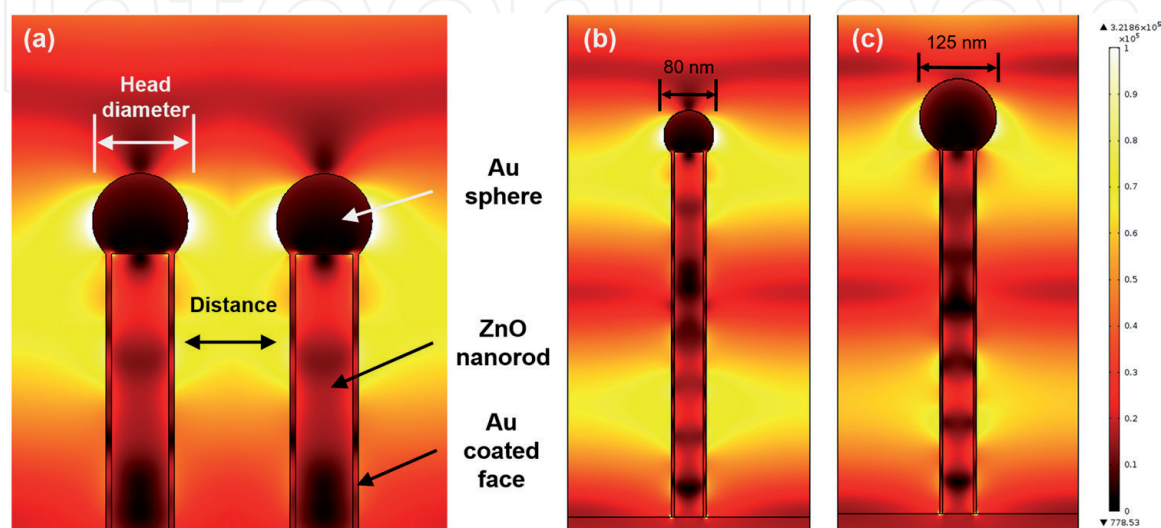


**Figure 4.** Finite element analysis showing (a) the different factor in LSPR on ZnO nanorod-based SERS substrates with gold head diameters of (b) 80 nm and (c) 125 nm, respectively.

600 nm. The near-field distribution of the electric fields was calculated for 785 nm incident light and parallel plate boundary conditions with symmetry of the electric field. Even if the head width is increased, there is almost no change in the full scale, and the electric field is distributed in the vertical direction of the incident light as shown in **Figure 4**. The cross-sectional width of incident light is 2  $\mu\text{m}$ , and the density of the nanorods in the region is constant. This suggests that the difference in SERS enhancement by Au thickness is due to concentration of sample at LSPR area.

## 5. Cell viability test

Raman measurements of nanometer-sized biomarkers secreted from living cells require confirmation of the suitability of cells for SERS substrates. The toxic endogenous properties of gold nanoparticles have previously been reported [29], and ZnO nanorods are reported to be toxic to NIH 3 T3 fibroblasts [30]. Therefore, it is necessary to confirm whether the sensing chip is suitable for cell application through the evaluation of cytotoxicity, and cell culture and cell viability tests were carried out as follows.

Breast cancer cell line of MDA-MB-231 was purchased from the Korean Cell Line Bank (Seoul, Korea). The breast cancer cells MDA-MB-231 were cultured in Dulbecco's modified Eagle's minimal essential medium (DMEM; Life Technologies, Inc., Grand Island, NY, USA) supplemented with 10% fetal bovine serum (FBS; Hyclone Laboratories, Logan, UT, USA) and a 1% penicillin–streptomycin solution (Life Technologies, Inc.) in a humidified 5% CO<sub>2</sub> incubator at 37°C. Cell viability analyses were based on MTT (Sigma, USA) assays. Cells were plated at a density of  $3 \times 10^5$  cells/well and incubated for 24 hours. After preparing the Au-ZnO substrate, the cell was treated with 5 mg/ml MTT for 30 min and then dissolved using DMSO. The absorbance was measured at 540 nm with an ELISA microplate reader (Multiskan EX, Thermo Scientific, USA). **Figure 5** shows the results of MTT assay of the death of the breast cancer cell line MDA-MB-231 according to SERS substrate condition. The MDA-MB-231 is commonly used in biotechnology applications such

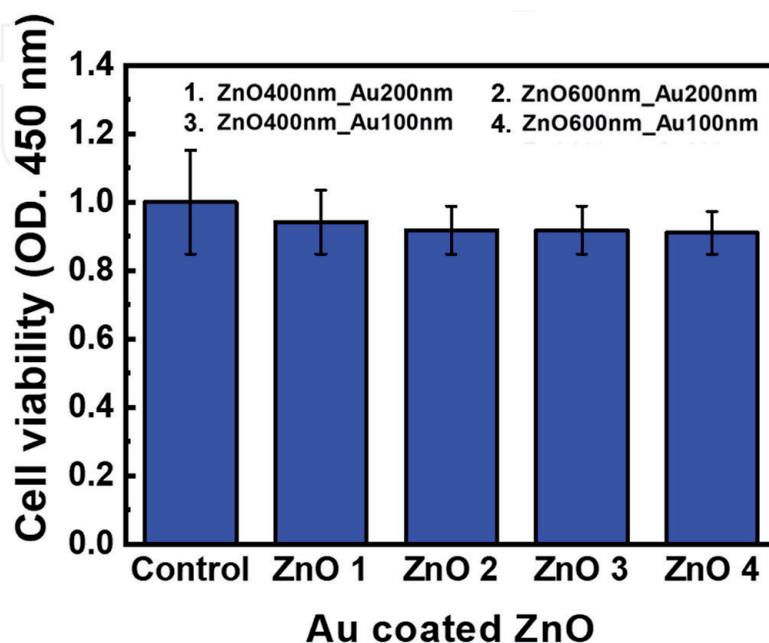


**Figure 5.**  
Cell viability of MDA-MB-231 on each substrate by MTT assay.

as analyzing cancer cell malignancy. From the results, the substrate at this ZnO nanorod and gold deposition conditions is suitable for experiments in live breast cancer cell lines.

## 6. Bio-application

Interstitial cystitis/bladder pain syndrome (IC/BPS) is a refractory disease that afflicts the vague pelvic pain when the urine enters the bladder and makes frequent urination [31]. There are various treatments based on oral agents [32–34], but they are still unsatisfactory with frequent recurrence of symptoms and Hunner's lesions [35]. Parallel with the development of therapeutic technology, early diagnosis of IC/BPS related to quality of life and detection of disease before development to chronic type can minimize patient's pain and increase treatment effect. Therefore, it is necessary to confirm the possibility of early detection of nanometer biomarkers from urine obtained from interstitial cystitis animal model using SERS substrate. IC/BPS animal models and comparative groups for these experiments were derived using 10-week-old female Sprague Dawley rats. The rats were instilled with 0.2 M HCl for 10 min using a 26-gauge angiocatheter in the bladders of four rats, followed by neutralization and saline wash. Other rats in the comparison group were used as vehicle instead of HCl injection. The voiding pattern was analyzed to confirm the reproducibility of animal modeling as in the previous paper [36]. Rat urine was collected in a 50 mL tube using a metabolic cage. The voiding pattern measured at a week after HCl injection was examined, and the collected urine was used as a sample for Raman measurement. Twenty-four hours of natural voiding patterns in the metabolic cage were recorded and analyzed using AcqKnowledge 3.8.1 software and an MP150 data acquisition system (Biopac Systems, Goleta, CA, USA) at a sampling rate of 50 Hz. The volume change of the obtained raw data of urine was estimated by 1 mL unit as shown in **Figure 6a**. Irregular frequency of urinary dysfunction caused by bladder inflammation is observed in HCl-treated rats and is consistent with previous animal model studies [35, 36]. Steps and terraces in the graph are the excretion urine and the duration between voiding, respectively. The total amount of control and IC/BPS animal models for approximately 10 hours is 11 and 13 mL, respectively. However, compared with the amount, the frequency is 3 and 6 times. When the unit of step is 0.5 mL, the frequency is 4 and 11 times, and the difference in the voiding frequency is clearly revealed.

From the identified sample, a drop of 5  $\mu\text{L}$  was applied to the SERS specimen, and the sample was allowed to spread for 60 min. After confirming that the droplets were dry and diffused, they were loaded onto a Raman spectroscope system attached to a microscope (IX-73, Olympus, Japan) and measured. As shown in **Figure 6b**, the diffused region of the sample can be confirmed by an optical microscope, and the region where the sample is diffused as in (c) can be confirmed to have a nanometer-scale porosity. In this area, Raman spectra were collected using a customized spectrometer (FEX-INV, NOST, Korea) with a 785 nm diode laser as the excitation source. The 1 mW of excitation light was focused on the sample through a 40  $\times$ /0.6 NA objective with spot size  $\sim 2.4 \mu\text{m}$ . The spectrum of each point was measured 8 times in the range of 550 to 1500  $\text{cm}^{-1}$  with a spectral resolution of 1  $\text{cm}^{-1}$  and an integration time of 40 s at room temperature. The Raman spectrum was calibrated by measuring a silicon sample before the Raman measurements. To evaluate the spectral differences between control and IC/BPS of rat urine, principal component analysis (PCA) was introduced. A statistical analysis method of PCA reduces the number of variables in multivariate systems, and all of spectral range was used as variables. All analyses were conducted using XLSTAT 2018 software.

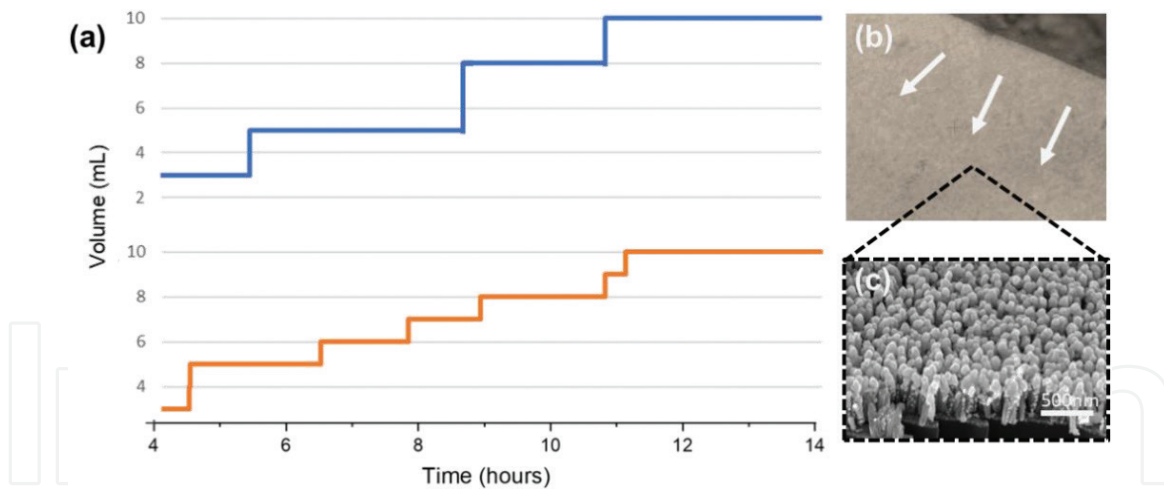


**Figure 6.**

(a) Measurement of voiding function in control group (blue line) and IC/BPS animal group (orange line) at 7 days after HCl treatment. (b) Optical microscope images of a Raman measurement region diffused from a sample droplet into a nanoporous area and (c) magnified SEM image.

As shown in **Figure 7a**, brown bars are indicated on the peak, which is the main factor above the graph drawn as the average of total data. The main peaks for the control and IP/BPS samples were observed at 641, 683, 723, 873, 1002, 1030, and 1355  $\text{cm}^{-1}$ , which corresponded to C-C twisting mode of tyrosine [37, 38], ring breathing of nucleic acids for G [38, 39] and A [39, 40], C-C stretch of hydroxyproline [37, 41], symmetric ring breathing mode [37–41] and C-H in-plane bending mode of phenylalanine [37, 41], and  $\text{CH}_3\text{CH}_2$  wagging mode of collagen [37, 41], respectively.

The peak at 1002  $\text{cm}^{-1}$  has a considerably large value compared to the rest of the data, which is notable in literature referring to other peaks, as they relate to other biologies. To analyze Raman peaks, PCA is utilized as shown in **Figure 7b**. Clear discrimination and reliable separation between control and IC/BPS groups were observed. By plotting PC2 and PC3, the groups show clear distinctions between IC/BPS urine and the control samples (dotted line). Raman spectrum measurements and PCA analysis showed that it is possible to distinguish between normal and diseased groups using gold-coated ZnO nanorod substrates that can be applied to early disease diagnostic sensing chips.

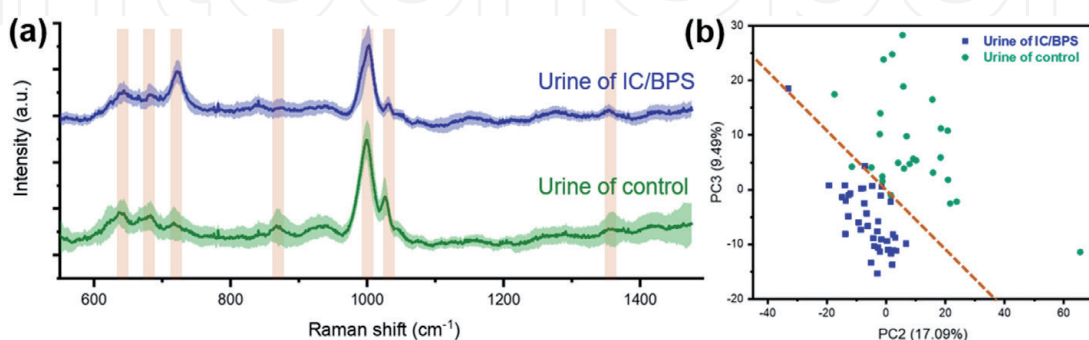


**Figure 7.**

(a) Averaged Raman spectra for IC/BPS (blue line) and control (green line) of rat's urine. Standard deviations are painted around the spectra. (b) Principal component analysis results for urine of IC/BPS and control sample.

## **7. Conclusion**

In summary, we compared the differences in surface-enhanced Raman effect using RhB by adjusting the length and diameter of ZnO nanorods and the volume of deposited gold in ZnO-based SERS substrates. Electron microscopy images showed clustering on top of nanorods during gold deposition and showed nanometer level porosity. As the volume of deposited gold increases, the Raman signal also improves, but as the growth conditions of the nanorods change, the signal intensity also changes. This is because the Raman enhancement factor is determined by the enhancement by the SERS properties of metal and the concentration of the sample. Through the finite element analysis in the two-dimensional plane, signal enhancement was similar for 80 and 125 nm of Au-grain head. It was found that the enhancement of the Raman signal was determined by the wider surface area of gold. It was confirmed that this signal enhancement is made in the vertical direction of the rod, so that only nanometer targets trapped in the porous space can obtain enhanced signals. In addition, the SERS chips based on ZnO nanorods were found to have no coffee ring effect in measuring liquid samples and were also suitable for cell application experiments. An IC/BPS animal model was constructed for the bio-application, the voiding pattern was observed for urinary disease status, and urine was collected from the IC/BPS. The obtained urine was diffused into a ZnO-based SERS chip having nanopores, and Raman was measured in the corresponding region. Statistical analysis of Raman signals obtained from nanometric level area showed that IC/BPS and normal animals were distinguished. Therefore, we can confirm that ZnO nanorod-based SERS has sufficient potential for early disease diagnosis by efficiently detecting nano-sized biomarkers.

## **Acknowledgements**

This work was supported by the Basic Science Research Program (2018R1D1A1B07048562) and MRC grant (2018R1A5A2020732) through the National Research Foundation of Korea (NRF) funded by the Ministry of Science and ICT (MSIT), by the Ministry of Trade, Industry and Energy (MOTIE) under the Industrial Technology Innovation Program (10080726, 20000843), and by a grant of the Korea Health Technology R&D Project through the Korea Health Industry Development Institute (KHIDI), funded by the Ministry of Health and Welfare, Republic of Korea (HI18C2391).

## **Conflict of interest**

The authors declare no conflict of interest.

IntechOpen

### Author details

Sanghwa Lee<sup>1</sup> and Jun Ki Kim<sup>1,2\*</sup>

<sup>1</sup> Biomedical Engineering Research Center, Asan Institute of Life Sciences, Asan Medical Center, Seoul, Republic of Korea

<sup>2</sup> Department of Convergence Medicine, University of Ulsan College of Medicine, Seoul, Republic of Korea

\*Address all correspondence to: kim@amc.seoul.kr

### IntechOpen

© 2019 The Author(s). Licensee IntechOpen. This chapter is distributed under the terms of the Creative Commons Attribution License (<http://creativecommons.org/licenses/by/3.0>), which permits unrestricted use, distribution, and reproduction in any medium, provided the original work is properly cited. 

## References

- [1] Ishigaki M, Maeda Y, Taketani A, Andriana BB, Ishihara R, Wongravee K, et al. Diagnosis of early-stage esophageal cancer by Raman spectroscopy and chemometric techniques. *Analyst*. 2016;**141**(3):1027-1033
- [2] Kikuchi H, Kawabata T, Okazaki S, Hiramatsu Y, Baba M, Ohta M, et al. Near-infrared multichannel Raman spectroscopy with a 1064-nm excitation wavelength for ex vivo diagnosis of gastric cancer. *Cancer Research*. 2011;**71**
- [3] Carvalho LFCS, Bonnier F, O'Callaghan K, O'Sullivan J, Flint S, Byrne HJ, et al. Raman microspectroscopy for rapid screening of oral squamous cell carcinoma. *Experimental and Molecular Pathology*. 2015;**98**(3):502-509
- [4] Lee SH, Kim OK, Lee S, Kim JK. Local-dependency of morphological and optical properties between breast cancer cell lines. *Spectrochimica Acta A*. 2018;**205**:132-138
- [5] Smith R, Wright KL, Ashton L. Raman spectroscopy: An evolving technique for live cell studies. *Analyst*. 2016;**141**(12):3590-3600
- [6] Liu TY, Tsai KT, Wang HH, Chen Y, Chen YH, Chao YC, et al. Functionalized arrays of Raman-enhancing nanoparticles for capture and culture-free analysis of bacteria in human blood. *Nature Communications*. 2011;**2**(538):1-8
- [7] Zhou HB, Yang DT, Ivleva NP, Mircescu NE, Niessner R, Haisch C. SERS detection of bacteria in water by in situ coating with Ag nanoparticles. *Analytical Chemistry*. 2014;**86**(3):1525-1533
- [8] Khatun Z, Bhat A, Sharma S, Sharma A. Elucidating diversity of exosomes: Biophysical and molecular characterization methods. *Nanomedicine-Uk*. 2016;**11**(17):2359-2377
- [9] Lee C, Carney RP, Hazari S, Smith ZJ, Knudson A, Robertson CS, et al. 3D plasmonic nanobowl platform for the study of exosomes in solution. *Nanoscale*. 2015;**7**(20):9290-9297
- [10] Maiti NC, Apetri MM, Zagorski MG, Carey PR, Anderson VE. Raman spectroscopic characterization of secondary structure in natively unfolded proteins: Alpha-synuclein. *Journal of the American Chemical Society*. 2004;**126**(8):2399-2408
- [11] Rygula A, Majzner K, Marzec KM, Kaczor A, Pilarczyk M, Baranska M. Raman spectroscopy of proteins: A review. *Journal of Raman Spectroscopy*. 2013;**44**(8):1061-1076
- [12] Stiles PL, Dieringer JA, Shah NC, Van Duyne RR. Surface-Enhanced Raman Spectroscopy. *Annual Review of Analytical Chemistry*. 2008;**1**:601-626
- [13] Etchegoin PG, Le Ru EC. A perspective on single molecule SERS: Current status and future challenges. *Physical Chemistry Chemical Physics*. 2008;**10**(40):6079-6089
- [14] Li WY, Camargo PHC, Lu XM, Xia YN. Dimers of silver nanospheres: Facile synthesis and their use as hot spots for surface-enhanced Raman scattering. *Nano Letters*. 2009;**9**(1):485-490
- [15] Wang YL, Irudayaraj J. Surface-enhanced Raman spectroscopy at single-molecule scale and its implications in biology. *Philos T R Soc B*. 1611;**368**:2013
- [16] Caldwell JD, Glembocki OJ, Bezares FJ, Kariniemi MI, Niinisto JT, Hatanpaa TT, et al. Large-area plasmonic hot-spot arrays: Sub-2 nm interparticle separations with plasma-enhanced

atomic layer deposition of Ag on periodic arrays of Si nanopillars. *Optics Express*. 2011;**19**(27):26056-26064

[17] Lee SJ, Morrill AR, Moskovits M. Hot spots in silver nanowire bundles for surface-enhanced Raman spectroscopy. *Journal of the American Chemical Society*. 2006;**128**(7):2200-2201

[18] Kleinman SL, Frontiera RR, Henry AI, Dieringer JA, Van Duyne RP. Creating, characterizing, and controlling chemistry with SERS hot spots. *Physical Chemistry Chemical Physics*. 2013;**15**(1):21-36

[19] Abu Hatab NA, Oran JM, Sepaniak MJ. Surface-enhanced Raman spectroscopy substrates created via electron beam lithography and nanotransfer printing. *ACS Nano*. 2008;**2**(2):377-385

[20] De Angelis F, Gentile F, Mecerini F, Das G, Moretti M, Candeloro P, et al. Breaking the diffusion limit with super-hydrophobic delivery of molecules to plasmonic nanofocusing SERS structures. *Nature Photonics*. 2011;**5**(11):683-688

[21] Cinel NA, Cakmakyapan S, Butun S, Ertas G, Ozbay E. E-Beam lithography designed substrates for surface enhanced Raman spectroscopy. *Photonic Nanostruct*. 2015;**15**:109-115

[22] Marotta NE, Barber JR, Dluhy PR, Bottomley LA. Patterned silver nanorod array substrates for surface-enhanced Raman scattering. *Applied Spectroscopy*. 2009;**63**(10):1101-1106

[23] Ngo YH, Li D, Simon GP, Gamier G. Paper surfaces functionalized by nanoparticles. *Adv Colloid Interfac*. 2011;**163**(1):23-38

[24] Li BW, Zhang W, Chen LX, Lin BC. A fast and low-cost spray method for prototyping and

depositing surface-enhanced Raman scattering arrays on microfluidic paper based device. *Electrophoresis*. 2013;**34**(15):2162-2168

[25] Zhang W, Li BW, Chen LX, Wang YQ, Gao DX, Ma XH, et al. Brushing, a simple way to fabricate SERS active paper substrates. *Anal Methods-Uk*. 2014;**6**(7):2066-2071

[26] Schmidt MS, Hubner J, Boisen A. Large area fabrication of leaning silicon nanopillars for surface enhanced Raman spectroscopy. *Advanced Materials*. 2012;**24**(10):Op11-Op8

[27] Albiss BA, AL-Akhras MA, Obaidat I. Ultraviolet photodetector based on ZnO nanorods grown on a flexible PDMS substrate. *Int J Environ an Ch*. 2015;**95**(4):339-348

[28] Chen Y, Tse WH, Chen LY, Zhang J. Ag nanoparticles-decorated ZnO nanorod array on a mechanical flexible substrate with enhanced optical and antimicrobial properties. *Nanoscale Research Letters*. 2015;**10**

[29] Ibupoto ZH, Khun K, Eriksson M, AlSalhi M, Atif M, Ansari A, et al. Hydrothermal growth of vertically aligned ZnO nanorods using a biocomposite seed layer of ZnO nanoparticles. *Materials*. 2013;**6**(8):3584-3597

[30] Sinha G, Depero LE, Alessandri I. Recyclable SERS substrates based on Au-coated ZnO nanorods. *Acs Appl Mater Inter*. 2011;**3**(7):2557-2563

[31] Tripp DA, Nickel JC, Wong J, Pontari M, Moldwin R, Mayer R, et al. Mapping of pain phenotypes in female patients with bladder pain syndrome/interstitial cystitis and controls. *European Urology*. 2012;**62**(6):1188-1194

[32] Evans RJ, Moldwin RM, Cossons N, Darekar A, Mills IW, Scholfield D. Proof

of concept trial of tanezumab for the treatment of symptoms associated with interstitial cystitis. *J Urology*. 2011;**185**(5):1716-1721

[33] Hanno PM, Erickson D, Moldwin R, Faraday MM. Diagnosis and treatment of interstitial cystitis/bladder pain syndrome: AUA guideline amendment. *J Urology*. 2015;**193**(5):1545-1553

[34] Nickel JC, Herschorn S, Whitmore KE, Forrest JB, Hu P, Friedman AJ, et al. Pentosan polysulfate sodium for treatment of interstitial cystitis/bladder pain syndrome: Insights from a randomized, double-blind, placebo controlled study. *J Urology*. 2015;**193**(3):857-862

[35] Kim A, Yu HY, Lim J, Ryu CM, Kim YH, Heo J, et al. Improved efficacy and in vivo cellular properties of human embryonic stem cell derivative in a preclinical model of bladder pain syndrome. *Sci Rep-Uk*. 2017;7

[36] Song M, Park J, Choo MS. Mesenchymal stem-cell therapy alleviates interstitial cystitis by activating Wnt signaling pathway. *J Urology*. 2015;**193**(4):E217-E21E

[37] Stone N, Stavroulaki P, Kendall C, Birchall M, Barr H. Raman spectroscopy for early detection of laryngeal malignancy: Preliminary results. *Laryngoscope*. 2000;**110**(10):1756-1763

[38] Synytsya A, Judexova M, Hoskovec D, Miskovicova M, Petruzela L. Raman spectroscopy at different excitation wavelengths (1064, 785 and 532 nm) as a tool for diagnosis of colon cancer. *Journal of Raman Spectroscopy*. 2014;**45**(10):903-911

[39] Chan JW, Taylor DS, Zwerdling T, Lane SM, Ihara K, Huser T. Micro-Raman spectroscopy detects individual neoplastic and normal hematopoietic cells. *Biophysical Journal*. 2006;**90**(2):648-656

[40] Wang H, Huang N, Zhao J, Lui H, Korbelik M, Zeng H. Depth-resolved in vivo micro-Raman spectroscopy of a murine skin tumor model reveals cancer-specific spectral biomarkers. *Journal of Raman Spectroscopy*. 2011;**42**(2):160-166

[41] Huang ZW, McWilliams A, Lui H, McLean DI, Lam S, Zeng HS. Near-infrared Raman spectroscopy for optical diagnosis of lung cancer. *International Journal of Cancer*. 2003;**107**(6):1047-1052